DIRECT DEPENDENCE BETWEEN TEMPERATURE, MICRO STRAINS AND STRUCTURAL DISTORTIONS IN NATURAL SiO_2 QUARTZ

Abdelhamid OUFAKIR[1,2], Lahcen KHOUCHAF [1], Mohamed AFQIR[2], Nabiha TAHIRI[2], Mohamed ELAATMANI[2], Abdelouahad ZEGZOUTI[2], Hassan El BAHRAOUI[2]

Elastic properties of silica depend on the temperature. In this work are reported the heat treatment effect on the structural behavior of natural SiO_2. X-ray diffraction (XRD), Transmission Electron Microscope and Fourier transform infrared spectroscopy are used to characterize natural SiO_2 before and after heat treatment samples. Williamson–Hall plots and Scherer's formula are applied to identify the crystallite sizes. The experimental results reveal the detailed modification while varying the temperature. Changes are revealed by FTIR spectra assigned to an amelioration in the structural order with increasing temperature is in good agreement with XRD and TEM analysis. Furthermore, the changes of crystallite sizes, microstructure, and the lattice parameters calculated from XRD data are strongly influenced by the heat treatment. Careful TEM images showed the nanograined for materials, which could be correlated to that estimated from Scherer's formula and Williamson–Hall plots.

Keywords: SiO_2 flint; Heat treatment; Microstructure; Crystallite size; Williamson–Hall

1. Introduction

Silicon dioxide or SiO_2 is a very abundant material in the Earth's crust. It exists in crystalline or amorphous form. Amorphous silica is generally of synthetic origin. SiO2 is an essential material in many industrial fields. It is used in construction materials such as cement and glass [1], it is important fillers in rubber [2], and it is used in pharmaceutical and medicine applications [3]. The surface composition, i.e., silanol and water contents of SiO_2 explain strongly its efficiency and usefulness [4]. The use of SiO_2 is principally due to the high surface area, the good dielectric and thermal properties. Moreover, SiO2 is inert which does not generate parallel reactions [5].

[1] IMT Lille Douai, Lille Université, Cité Scientifique, Rue Guglielmo Marconi, BP 20145, 59653 Villeneuve D'Ascq Cedex–France

[2] Laboratoire Sciences des Matériaux Inorganiques et leurs Applications, faculté des Sciences Semlalia, Cadi Ayyad University, BP 40000, Marrakech–Morocco

Upon heating, the trigonal a-quartz existing at normal temperature will transform into hexagonal b-quartz at 573°C. Temperature influences the structure by, only, modifying the angles and the lengths of the Si-O-Si bonds [6-7]. The silanol-group concentration decreases at higher treatment temperature by dehydroxylation processes through which two silanol OH groups are released by forming a water molecule and siloxane bonds according to the reaction (1) [8-9]:

$$2Si\text{-}OH \rightarrow Si\text{-}O\text{-}Si + H_2O \quad (1)$$

The lattice strain and crystallite size would change the intensity and the position of the 2θ peak [10]. Therefore, the lattice strain and crystallite size can be obtained by analyzing the peak width. The crystallite size is different from the particle size owing to the presence of polycrystalline aggregates [11]. Lattice strain is slight displacements of atoms relative to their normal lattice positions, arising from crystal imperfections such as dislocations, contract or sintered stresses and interstitial and impurity atoms [12]. The Scherer's formula is used in the determination crystallite size when there is no strain on the materials [13]. The Williamson–Hall (W–H) analysis is employed for estimating lattice strain and crystallite size of nanomaterials [14, 15].

Previous studies [16-19] reported that the crystallite size determined from XRD data using Scherer's formula and Williamson–Hall analysis was in good agreement with that obtained by Transmission Electron Microscope.

The elastic properties define the hardness and strength of materials and significantly affect the thermal shock behavior of materials. There are different analytical techniques that can estimate the microstructural properties of materials [20-23]. To our knowledge, it does not resolve much physical issues leading to the change of the structural properties of SiO_2 materials.

This paper investigates the effect of heat treatment on the microstructure morphology of SiO_2 flint by Scherer's formula and Williamson–Hall plots methods. The lattice strain was estimated using a modified form of Williamson–Hall methods such as uniform deformation model (UDM), uniform deformation stress model (UDSM) and uniform deformation energy density model (UDEDM).

2. Experimental

The material used in this work is a natural SiO_2 flint from the north of France; we study two states of flint; raw flint and a heat-treated flint at 650 °C. The procedure of heat treatment is as follows: The siliceous natural aggregate was heated in a furnace at 100 °C during 24h and then at rate 5 °C/min to rise up to 650 °C and kept to this temperature for 1 hour.

The X-ray diffraction (XRD) measurements were carried out using a Shimadzu Bruker D8 Advance diffractometer (Cu-Kλ radiation = 1.5418 Å),

operating at 40 kV and 40 mA. Data were recorded in the range of 25°–75° in the 2θ scale with a step size of 0.02° and a counting time of 0.5s/step.

The Transmission Electron Microscope investigations were performed with a FEI Tecnai G2-20 instrument with an accelerating voltage of 200 kV. It is equipped with a filament of lanthanum hexaboride LaB6, a double-tilt holder and Gatan digital camera CCD ORIUS.

The Fourier transform infrared spectroscopy (FTIR) were recorded by Brucker VERTEX 70 spectrometer in reflection mode, by collecting 100 scans at 4 cm^{-1} resolution in the range of 400–5000 cm^{-1}.

3. Results and discussion

3.1 XRD analysis

The X-ray diffraction analysis of natural and heated SiO_2 samples presented in Fig 1, shows that all samples have got the SiO_2 quartz structure with space group P312 (JCPDS-file 00-001-0649).

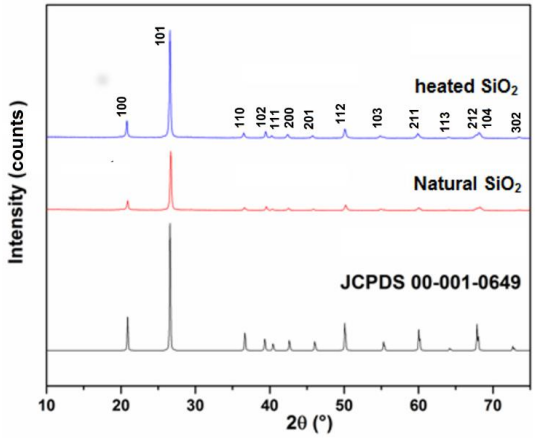

Fig. 1. XRD patterns of SiO_2 samples before and after heat treatment

Table 1 summarized the XRD lattice parameters. The volume increases between natural SiO_2 flint and heated ones is about 0.6%. This increased of lattice parameters could be linked to the formation of a crystalline phase from an amorphous.

Table 1

XRD data parameters of SiO_2 samples.

Samples	a (Å) = b (Å)	c (Å)	Cell volume ($Å^3$)
Natural SiO_2	4.8983±0.0003	5.3870±0.0007	111.940±0.01
Heated SiO_2	4.9064±0.0003	5.3997±0.0007	112.571±0.01

Thus, it usually can be described in terms of "long-range order" or "close packing", That's why the density of crystalline phase will be maximal under 650°C. The crystallite size of natural and heated SiO_2 samples was determined using the Debye–Scherer formula (2):

$$D_{D-S} = \frac{0.9\lambda}{\beta cos\theta} \quad (2)$$

Where $D_{D\text{-}S}$ is crystallite size, λ=1.5406 Å and β is Full-Width Half-Maximum [24]. The results show that crystallite size increased from 63 nm for natural SiO_2 flint to 70 nm for heated SiO_2 sample when applied at the highest reflection peak (101). This may be explained as the improved crystalline quality of the heated SiO_2.

In order to understand the contributions of lattice strain and crystalline size to the XRD peaks, different form of Williamson–Hall methods such as isotropic strain model, anisotropic strain model and uniform deformation energy density model is used.

The lattice isotropic strain (ε) and crystallite size ($D_{W\text{–}H}$) is given by isotropic strain model (equation 3):

$$\beta cos\theta = \frac{0.9\lambda}{D_{W-H}} + 4\varepsilon sin\theta \quad (3)$$

Fig. 2 shows ($\beta cos\theta$) as a function of ($4sin\theta$) of SiO_2 samples. The strains (ε) present in the materials and the crystallite size ($D_{W\text{–}H}$) are, respectively, obtained from the slope and from the $\beta cos\theta$-intercept of graph.

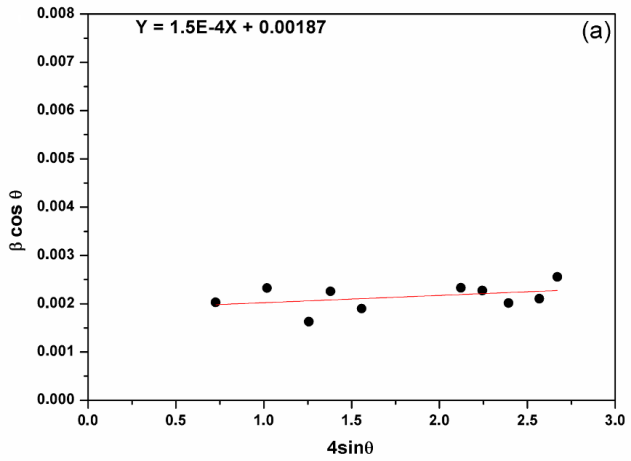

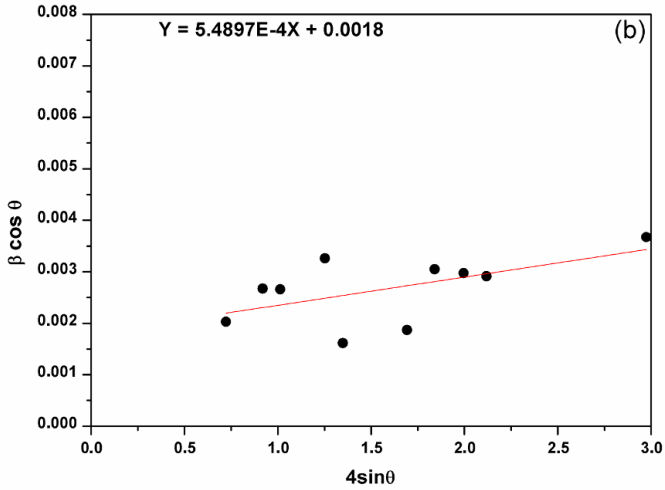

Fig. 2. Williamson-Hall plots of (a) natural and (b) heated SiO_2 samples.

The plotted graph clearly indicates the positive strain of natural and heated SiO_2 samples. The microstrain, which has been estimated at 1.50×10^{-4} units for natural SiO_2, is smaller than of heated SiO_2 which is 5.49×10^{-4} units. The average crystallite size is 73 nm, 77 nm for natural and heated SiO_2 samples respectively. These particle size values appear to be in good agreement with the one calculated by Scherer formula. In many cases, material cannot be having identical values of a property in all directions. The stress-strain relationships for elastic behavior are described by Hooke's law, which is valid only up to the proportionality limit of a material. Beyond this limit, Hooke's law no longer applies. Williamson-Hall equation (3) could be written by another way:

$$\beta cos\theta = \frac{0.9\lambda}{D_{W-H-ASM}} + \frac{4\sigma sin\theta}{Y_{hkl}} \tag{4}$$

Where σ is uniform stress and Y_{hkl} the Young's Modulus in the direction perpendicular to the set of crystal lattice planes (hkl). Equation (5) is the formula used to calculate Young Modulus in Hexagonal system [18]:

$$Y_{hkl} = \frac{\left[h^2 + \frac{(h+2k)^2}{3} + \left(\frac{al}{c}\right)^2\right]^2}{s_{11}\left(h^2 + \frac{(h+2k)^2}{3}\right)^2 + s_{33}\left(\frac{al}{c}\right)^4 + (2s_{13} + s_{44})\left(h^2 + \frac{(h+2k)^2}{3}\right)\left(\frac{al}{c}\right)^2} \tag{5}$$

where the Young's Modulus Y_{hkl} can be determined along any orientation, from the elastic constants (s_{ij}).

The elastic parameters of the compliance coefficients for SiO_2 [25] are s_{11}=0.01149 GPa^{-1}, s_{33}=0.00943 GPa^{-1}, s_{13}=0.08333 GPa^{-1} and s_{44}=0.01754 GPa^{-1}.

A scatter plot with a regression line of $\beta\cos\theta$ versus $4\sin\theta/E$ is plotted in Fig. 3, where (σ) is the slope of the line, and ($k\lambda/D_{W\text{-}H\text{-}ASM}$) is the $\beta\cos\theta$-intercept. In this situation, $\beta\cos\theta$ tends to increase as $\sin\theta$ increases, implying a positive correlation. The crystallite size ($D_{W\text{-}H\text{-}ASM}$) is 68 nm for natural SiO_2 and 69 nm for heated SiO_2. The magnitude of the deformed stress (σ) is found at around 122.804 MPa for natural SiO_2 and 103.159 MPa for heated SiO_2. Evidence for this comes from previous work showing that Young's modulus decreases with increase in temperature [26, 27, and 28].

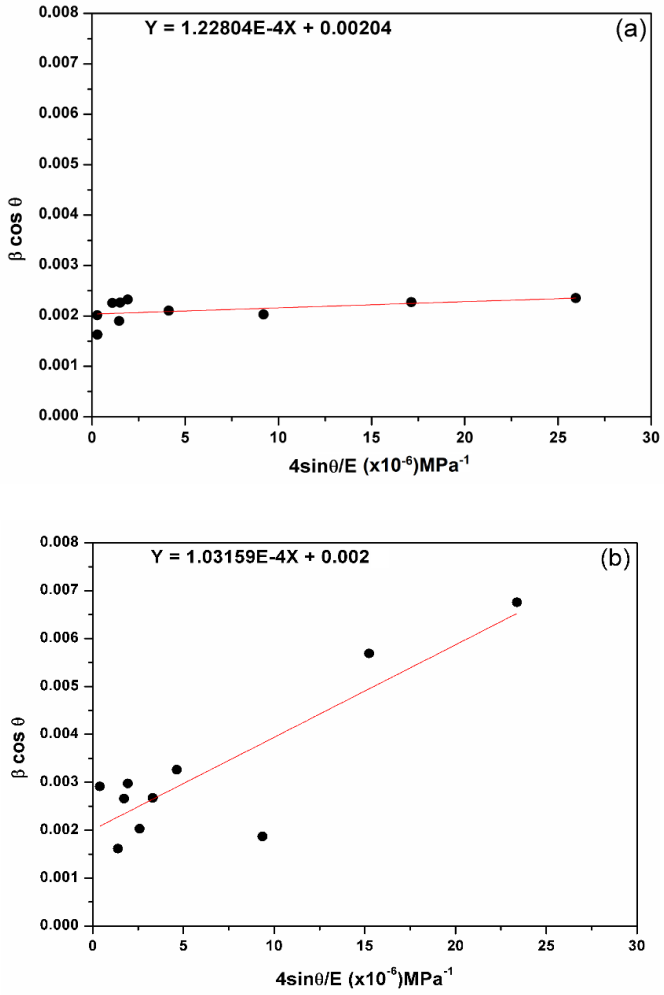

Fig. 3. Williamson-Hall plots with Young's modulus of (a) natural and (b) heated SiO_2 samples.

Here, the introduction of the anisotropic Young's modulus does not bring significant change on the scatter of data points. We can use another model, called the Uniform Deformation Energy Density Model (UDEDM), to determine the

energy density of a crystal. Moreover, to extend the anisotropic approach, Hooke's law can therefore also be interpreted as a relation between the strain (ε) and the energy density u (energy per unit volume):

$$u = \frac{\varepsilon^2 E}{2} \tag{6}$$

The relationship of equation (3) can be rewritten according the energy and strain relation as following:

$$\beta cos\theta = \frac{k\lambda}{D_{W-H-EDM}} + 4sin\theta \sqrt{\left(\frac{2u}{E}\right)} \tag{7}$$

The graph drawn between $\beta cos\theta$ and $4sin\theta/(E/2)^{1/2}$ is shown in Fig. 4.

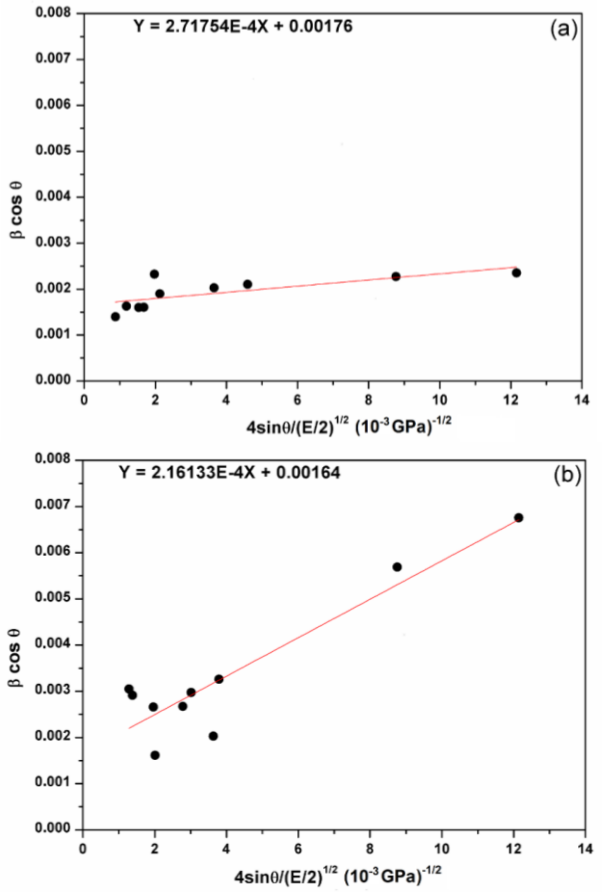

Fig. 4. Williamson-Hall plots with deformation energy density of (a) natural and (b) heated SiO_2 samples.

Using the regression equation to calculate slope and intercept, the crystallite size ($D_{W\text{-}H\text{-}EDM}$) remains almost closer to the obtained ones by Scherer method

(equation 1). The deformation energy density (u) is estimated to be 73.85 kJ/m^3 and 46.71 kJ/m^3 for natural and heated SiO_2 samples respectively. In our case, all the three models give the similar order of the crystallite size, which means that the strain has little effect on of the crystallite size.

3.1 TEM analysis

TEM technique one of the best techniques for nanoparticle size measurements. In this section, TEM is used to characterize the particles size change under heat treatment. Fig. 5 shows MET image of natural and heated SiO_2 samples. For natural SiO_2 flint (fig5. a), geometrical grains and angular sides characterizing angles of quartz are observed with average size 60 nm – 80 nm. Meanwhile, the MET did not rule out the presence of hexagonal crystals. Instead of heated SiO_2 (fig5. b), the morphology was found to be clearly dominated by the presence of hexagonal crystals, with grain size around 68 nm – 75 nm.

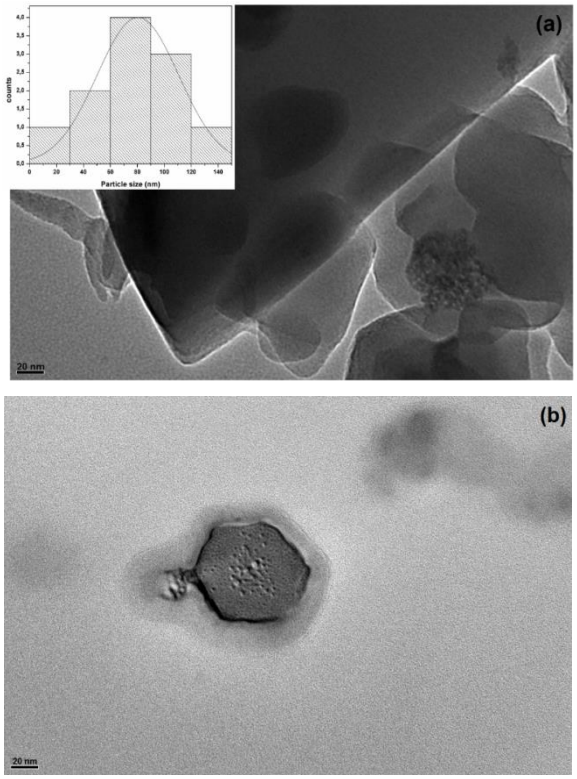

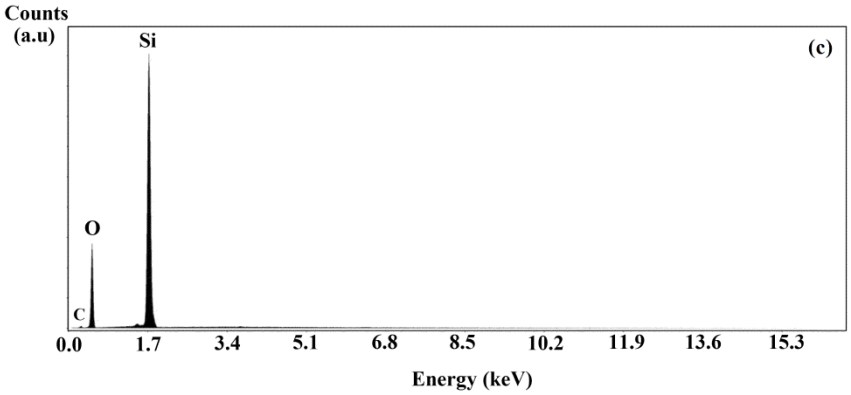

Fig. 5. TEM images of (a) natural, (b) heated SiO_2 samples and (c) EDS spectra of natural flint. The size distribution of the SiO_2 was shown in inset.

As shown in Fig. 5 the average size calculated from the TEM analysis is in good correlation with the results obtained from the powder XRD measurements. Fig. 5.c shows the EDS analysis corresponding to natural SiO_2 sample. We observe the presence of Si and O elements characteristic of SiO_2 compound. The presence of carbon is due to the sample holder.

The results obtained from the Scherer method, UDM, USDM, UDEDM, and TEM analysis are summarized in Table 2. The values of average crystallite size of natural and heated SiO_2 samples obtained from the different models are more or less similar, implying that the inclusion of strain in various forms has a very small effect on the average crystallite size of SiO_2 samples

Table 2.

Geometric parameters of natural and heated SiO_2 samples.

Models	Parameters	Natural SiO_2	Heated SiO_2
Scherer method	$D_{D\text{-}S}$ (nm)	63	70
Isotropic strain model	$D_{W\text{-}H}$ (nm)	73	77
	ε (No unit)	$1.5*10^{-4}$	$5.48*10^{-4}$
Anisotropic strain model	$D_{W\text{-}H\text{-}ASM}$ (nm)	68	73
	σ (MPa)	122.80	103.16
Uniform Deformation Energy Density model	$D_{W\text{-}H\text{-}EDM}$ (nm)	79	83
	u (kJ/m^3)	73.85	46.71
TEM analysis	D (nm)	61	72

3.3 FTIR analysis

Fig. 6 shows FTIR spectral patterns of unheated and heated flints between 400 cm^{-1} and 1400 cm^{-1}. Two strong peaks located at 1078 cm^{-1} and 1163 cm^{-1}

could be attributed to Si–O–Si stretching vibrations. Moreover, they show the presence of the double peak at 797–778 cm^{-1}, band at 693 cm^{-1} and two bands at 509-455 cm^{-1}, which are attributed to O–Si–O bending vibrations [29]. The band at 555 cm^{-1} is assigned to Si-O bending vibrations of no bridging Si-OH bonds and the band at 950 cm^{-1} is ascribed to stretching vibration.

The spectrum of heated flint clearly shows a reduction in the intensity of the 950-555 cm^{-1}, and a rise in the intensity of the bands located at 455 - 797 cm^{-1} reflecting a loss of some silanols groups and formation of new bridging Si-O-Si according to the reaction (1). In addition, we can notice the increase of the intensity of the double peak located at 797–778 cm^{-1}, which is related to presence of crystalline phase.

The principal band is shifted from 1078 cm^{-1} to 1082 cm^{-1}. According to previous studies [30], the more the structure is ordered, the more this band is located at the large wave numbers. This means that the shift of this band may be attributed to an improvement in structural order with increasing temperature in good agreement with XRD and TEM analysis.

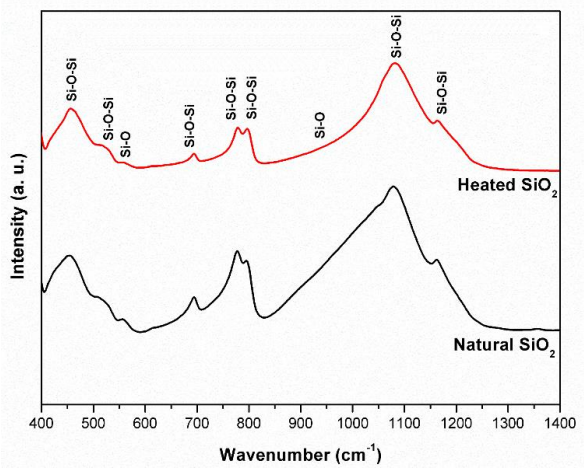

Fig. 6. FTIR spectra of the SiO_2 samples.

A heat-treatment at 650°C does not require in elimination of the water. The subsequent heat treatment leads molecular rearrangements occur to produce the appropriate crystalline structures. Thus, a heat treatment of natural silica causes the formation of Si-O-Si bond [31]. Moreover, the increase of crystallite size could be linked to a reduction of defects and structural distortions [32].

Based on these results, we can conclude that silanols Si-OH defects are decreased and the crystalline quality is improved with heat treatment.

4. Conclusion

The effect of annealing of SiO_2 flint has been reported. X-ray diffraction peak broadening analysis by Scherer method and Williamson Hall plots were used

to estimate the crystallite size, in order to correlate it with FTIR and MET analysis. However, The TEM results are in close correlation with the results of the XRD data. A change of the FTIR band assigned to an amelioration in the structural order with increasing temperature is in good agreement with XRD and TEM analysis. Based on the above it seems that crystallinity develops with heat treatment up to 650°C arising from a direct temperature dependence on the number of defects, global order and structural distortions.

R E F E R E N C E S

[1]. *T. Oertel, F. Hutter, U. Helbig, G. Sextel,* Amorphous silica in ultra-high-performance concrete: First hour of hydration. Cement and Concrete Research 58 (2014) 131-142.

[2]. *Y. W. Ngeow, J. Y. Y. Heng, D. R. Williams, R. T. Davies, K. M. E. Lawrence, and A. V Chapman*. Journal of Rubber Research. 22 (2019) 1–12.

[3]. *A. Libermana, N. Mendeza, W. C. Troglerb, A. C. Kummel*, Synthesis and surface functionalization of silica nanoparticles for nanomedicine, Surface Science Reports 69 (2014) 132–158

[4]. *J. P. Gallas, J. M. Goupil, A. Vimont, J. C. Lavalley, B. Gil, J. P. Gilson and O. Miserque,* Quantification of water and silanol species on various silicas by coupling IR spectroscopy and in-situ thermogravimetry, Langmuir. 25 (2009) 5825–5834.

[5]. *M.A.T.M. Broekmans*. Structural properties of quartz and their potential role for ASR. Materials Characterization. 53 (2004) 129–140.

[6]. M. Földvári, Handbook of the thermogravimetric system of minerals and its use in geological practice, 56 (2011).

[7]. D. K. Oopmann, B. Ag, and F. Republic, Selenium and selenium compounds. IARC Monogr. Eval. Carcinog. Risk Chem. Man, 9 (2010) 245–260, 1975.

[8]. H. E. Bergna, W. O. Roberts, Colloidal Silica: Fundamentals and Applications, CRC Taylor & Francis, 2006.

[9]. *P. Van Der Voort, I. Gillis-D'Hamers, K. C. Vrancken and E. F. Vansant*, Effect of Porosity on the Distribution and Reactivity of Hydroxyl Groups on the Surface of Silica Gel, J. Chem. Soc. Faraday Trans. 87 (1991) 3899-3905.

[10]. *B. Holm and R. Ahuja,* Ab initio calculation of elastic constants of SiO2 stishovite and α-quartz, J. Chem. Phys. 111 (1999) 2071–2074.

[11]. E. *M. Arruda, S. Ahzi, Y. Li, and A. Ganesan*, Rate Dependent Deformation of Semi-Crystalline Polypropylene Near Room Temperature, J. Eng. Mater. Technol., 119 (1997), 216.

[12]. J.M. Zhang, Y. Zhang, K.W. Xu, V. Ji, General compliance transformation relation and applications for anisotropic hexagonal metals, Solid State Communications 139 (2006) 87–91.

[13]. *B.D. Cullity*, Elements of X-ray diffraction, Second ed, London, UK: Addision Wesley, 1978.

[14]. *S. D. Bakshi, D. Sinha, S. G. Chowdhury*, Anisotropic broadening of XRD peaks of α-Fe: Williamson-Hall and Warren-Averbach analysis using full width at half maximum (FWHM) and integral breadth (IB). Materials Characterization (2018).

[15]. *S. Sivasankaran*. X-ray peak broadening analysis of AA 6061_{100-x}−x wt.% Al_2O_3 nanocomposite prepared by mechanical alloying. Materials characterization 62 (2011) 661-672.

[16]. *V. Uvarov, I. Popov*, Metrological characterization of X-ray diffraction methods for determination of crystallite size in nano-scale materials. Materials characterization 27 (2007) 883–91.

[17]. *A. Ghasemi, D. Penther, S. Kamrani,* Microstructure and nanoindentation analysis of Mg-SiC nanocomposite powders synthesized by mechanical milling. Materials Characterization 142 (2018) 137–143.

[18]. *G. Dirras, J. Gubicza*, A. Heczel, L. Lilensten, J-P. Couzinié, L. Perrière, I. Guillot, A. Hocini, Microstructural investigation of plastically deformed $Ti_{20}Zr_{20}Hf_{20}Nb_{20}Ta_{20}$ high entropy alloy by X-ray diffraction and transmission electron microscopy, Materials Characterization (2015).

[19]. *A. Maurya, P. Chauhan*, Structural and optical characterization of CdS/TiO_2 nanocomposite. Materials Characterization 62 (2011) 382–390.
[20]. P. Scherrer, Bestimmung der Grösse und der inneren Struktur von Kolloidteilchen mittels Röntgenstrahlen, Nachr. Ges. Wiss. Göttingen, Math.-Phys. Kl. 1918 (1918) 98–100.
[21]. *G.K.Williamson, W.H. Hall*, X-ray line broadening from filed aluminiumand wolfram, Acta Metall. 1 (1953) 22–31.
[22]. *K. Santra, P. Chatterjee, S. P. Sen Gupta*. Voigt modelling of size-strain analylsis: applicaton to α-Al_2O_3 prepared by combustion technique. Bulletin of Material Science. 25 (2002) 251–257.
[23]. *Y.T. Prabhu, K. Venkateswara Rao, V. Sesha Sai Kumar, B. Siva Kumari,* X-ray analysis of Fe doped ZnO nanoparticles by Williamson-Hall and size-strain plot. International Journal of Enginering and Advanced Technology. 2 (2013) 268-274.
[24]. *M.L.Dinesha, G.D. Prasanna, C.S. Naveen, H.S. Jayanna,* Structural and dielectric properties of Fe doped ZnO nanoparticles. Indian J. Phys. 87 (2013) 147–153.
[25]. *B.D. Cullity, S.R. Stock*, Elements of X-Ray Diffraction, 3rd edn. Prentice-Hall, New Jersey (2001).
[26]. *A. Khorsand Zak, W. H. Abd. Majid, M. E. Abrishami, and R. Yousefi*, X-ray analysis of ZnO nanoparticles by Williamson-Hall and size-strain plot methods, Solid State Sci. 13 (2011) 251–256.
[27]. *W. Pabst and E. Gregorová*, Elastic Properties of Silica Polymorphs, Ceramics – Silikáty 57 (2013) 167-184.
[28]. *J.Wang, Q-A Huang and H. Yu*, Size and temperature dependence of Young's modulus of a silicon nano-plate, J. Phys. D: Appl. Phys. 41 (2008) 165406. https://doi.org/ 10.1088/0022-3727/41/16/165406.
[29]. *T. Oh and C. K. Choi*, Comparison between SiOC Thin Film by plasma enhance chemical vapor deposition and SiO_2 Thin Film by Fourier Transform Infrared Spectroscopy, J. Korean Phys. Soc., 56 (2010) 1150–1155.
[30]. *N. Tahiri, L. Khouchaf and M. Elaatmani,* Durability performance of concrete with heat treatment of SiO2 aggregate. Int. J. Eng. Sci. Innov. Technol., 4 (2015) 55–62.
[31]. *N. Tahiri, L. Khouchaf, M. Elaatmani, G. Louarn, A. Zegzouti, and M. Daoud,* Study of the thermal treatment of SiO2 aggregate, IOP Conf. Ser. Mater. Sci. Eng., 62 (2014).
[32]. *M. Strauss, C. M. Maroneze, J. M. De Souza E Silva, F. A. Sigoli, Y. Gushikem, and I. O. Mazali,* Annealing temperature effects on sol-gel nanostructured mesoporous TiO_2/SiO_2 and its photocatalytic activity, Mater. Chem. Phys. 126 (2011) 188–194.